JOURNAL OF APPLIED PHYSICS **117**, 163915 (2015)

The atomic details of the interfacial interaction between the bottom electrode of $Al/AlO_x/Al$ Josephson junctions and HF-treated Si substrates

L. J. Zeng,[1] P. Krantz,[2] S. Nik,[1] P. Delsing,[2] and E. Olsson[1]
[1]*Department of Applied Physics, Chalmers University of Technology, 412 96 Gothenburg, Sweden*
[2]*Department of Microtechnology and Nanoscience, Chalmers University of Technology, 412 96 Gothenburg, Sweden*

(Received 25 February 2015; accepted 16 April 2015; published online 28 April 2015)

The interface between the Al bottom contact layer and Si substrates in Al based Josephson junctions is believed to have a significant effect on the noise observed in Al based superconducting devices. We have studied the atomic structure of it by transmission electron microscopy. An amorphous layer with a thickness of ~5 nm was found between the bottom Al electrode and HF-treated Si substrate. It results from intermixing between Al, Si, and O. We also studied the chemical bonding states among the different species using energy loss near edge structure. The observations are of importance for the understanding of the origin of decoherence mechanisms in qubits based on these junctions. © *2015 Author(s). All article content, except where otherwise noted, is licensed under a Creative Commons Attribution 3.0 Unported License.*
[http://dx.doi.org/10.1063/1.4919224]

I. INTRODUCTION

Tremendous progress has been made in implementing quantum bits (qubits) in superconducting integrated circuits incorporating Josephson junctions with the aim to achieve quantum information processing.[1–5] It has been demonstrated that coherent quantum states in the circuits can be manipulated and read out for quantum computation.[6–13] Long coherence time of those states is essential for the realization of quantum computation utilizing superconducting qubits. Thus, decoherence in the superconducting circuits based on Josephson junctions has been considered as a major obstacle for the application of quantum computing, as it can cause energy dissipation and destroy the coherent quantum states in the devices. The main source of decoherence has been found to be the coupling between the qubits and the environment surrounding it.[14–16] The device may couple to the external space via electromagnetic interaction. These direct electromagnetic interactions between the superconducting quantum devices and the outside world can be minimized by filtering and shielding. The coherence time of the quantum state in superconducting devices has been significantly improved over the last few years by optimizing the design of the superconducting circuits and improving the measurement techniques.[17–20] At the material component level, the interaction between the qubits and the dielectric substrate they sit on is also found to contribute significantly to the decoherence in superconducting quantum devices.[14,16] Such interaction is material structure dependent and will become the limiting factor for elevating the coherence time further when the decoherence at the device design level has been successfully suppressed.

Different physical models have been employed to describe the interaction between the qubits and the dielectric substrate. It has been concluded that the two-level fluctuators (TLF) in an amorphous dielectric can disrupt the coherence of Josephson qubits fabricated on amorphous substrates.[16] It has also been proposed that localized metal-induced gap states (MIGS) at the qubit/substrate interface can cause flux noise, which results in decoherence in quantum qubits.[21] However, to get a clear picture about the contribution and effect of interaction between the states in qubits and the dielectric substrates in a superconducting quantum device, it is critical to first have a comprehensive understanding of the microstructure at the qubit/substrate interface.

Single crystalline Si and amorphous SiO_2 (thermally grown on Si wafer, usually with a thickness of a few hundred nanometers) are the common substrates for the fabrication of Josephson junctions. The microstructural interaction between the Al based Josephson junctions and the SiO_2 substrate has been investigated in a previous study.[22] In this study, we focus on the structure at the interface between $Al/AlO_x/Al$ Josephson junction and silicon substrate, more specifically, at the Al/Si (HF-treated) interface. $Al/AlO_x/Al$ Josephson junctions fabricated on Si wafer are widely used in superconducting electronics due to the simplicity of the fabrication process and its compatibility with the fabrication techniques already implemented in silicon industry. By using transmission electron microscopy (TEM), we studied the detailed structure at the qubit/substrate interface with atomic resolution. Previously, the reaction and interaction between Al and Si have been studied by various techniques in systems made under different conditions.[23–26] However, there are few detailed investigations on the interface structure in the qubit system with atomic resolution.

II. MATERIALS AND METHODS

The $Al/AlO_x/Al$ tunnel junctions were deposited on Si substrates. The Si wafer was HF etched (etched for 1 min with 2% HF, then dipped in de-ionized water for 20 s) prior to evaporation with the intention to remove the native oxide on the surface of the wafer. Both the bottom and the top Al electrode layers were electron beam deposited at a rate of

 © Author(s) 2015

about 5 Å/s. After deposition of the bottom Al layer, O_2 was let in to the deposition chamber, and the pressure of the gas was dynamically regulated to be 0.2 mbar. The oxidation process took 30 min and resulted in a thin AlO_x film on the surface of the Al layer. The top Al electrode was then deposited after the formation of aluminum oxide barrier. The nominal thicknesses of the bottom and top Al layers were 35 nm and 55 nm, respectively. Unpatterned samples were used in our study.

Cross-section TEM samples were prepared by mechanical polishing and dimpling followed by Argon ion milling to electron transparency. An FEI Titan 80–300 TEM/Scanning TEM (STEM) with a probe C_s corrector and a Gatan Imaging Filter (GIF) Tridium was used for high resolution imaging, electron energy loss spectroscopy (EELS), and energy filtering transmission electron microscopy (EFTEM). Annular dark field (ADF) STEM images were acquired using a 19.7 mrad beam convergence angle and ~54–270 mrad detector collection angle.

III. RESULTS AND DISCUSSION

Figs. 1(a) and 1(b) show the images taken at the Al/Si (HF-treated) interface in an Al/AlO_x/Al junction fabricated on a Si substrate. Fig. 1(a) is a TEM bright field (BF) image, and Fig. 1(b) is a STEM ADF image. In Fig. 1(a), lattice fringes from Al and Si layers are clearly visible. From Fig. 1(a), we can also clearly see that there is an interfacial layer existing between the bottom Al layer in the junction and the single crystalline Si substrate. The thickness of the interfacial layer is around 5 nm. Based on the results from both the TEM imaging and electron nano-diffraction performed at the interfacial layer, we conclude that this layer is amorphous. Fig. 1(b) also shows that the bottom Al layer is not in direct contact with the single crystalline Si substrate. The distance between the bottom surface of the Al layer and the top surface of the Si substrate is about 5 nm. Moreover, we found that there is an intensity variation within the interfacial layer in STEM ADF images, while the intensity of the interfacial layer in TEM BF images is more homogeneous. According to the contrast in the STEM ADF images, we describe the layer as consisting of two parts, marked as area I and II in Fig. 1(b). STEM ADF imaging is an incoherent imaging technique because of the fraction of electrons that are collected by detector in this imaging mode. By collecting the transmitted electrons scattered to large angles, namely, Rutherford scattered electrons, the intensity of STEM ADF images is atomic number (Z) dependent. Thus, STEM ADF images are more sensitive to the chemical composition of the material as compared to TEM BF images. The contrast variation across the interfaces in Fig. 1(b) indicates not only the existence of the interfacial layer at Al/AlO_x/Al junction and Si substrate interface but also a change of the local chemical composition and structure within the interfacial layer.

In order to examine the distribution of different elements at the interface, it was also studied using EFTEM. Fig. 2 shows the elemental maps acquired with Al L-edge, O K-edge, and Si K-edge. As shown in Fig. 2(a), the Al map, the bright region represents the Al-rich area in the material. There are three distinct areas with different intensity in the image, indicating areas with different Al concentrations. In between the Al-rich (Al electrode) and the Al-free (Si substrate) layers, there exists a layer with lower Al concentration when compared to the Al-rich layer but higher concentration than the Al-free layer, and with the thickness of around 5 nm. A comparison with the TEM BF image (e.g., Fig. 1(a)) shows that this layer with intermediate Al concentration is the interfacial layer between the bottom Al electrode and Si substrate. Similarly, in Si maps, the Si signals not only exist in the Si substrate area, but also extend into the interfacial layer, as shown in Fig. 2(c). In addition to Al and Si, O was also found in this interfacial layer, as

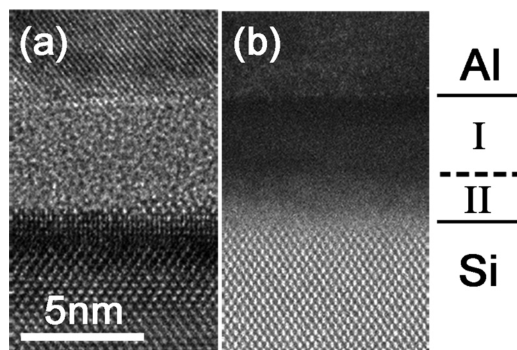

FIG. 1. BF TEM image (a) and ADF STEM image (b) taken at the interface between the Al/AlO_x/Al tunnel junction and the Si substrate. An interfacial layer is clearly visible in both images. The positions of Al, Si, and area I and II are also illustrated based on the contrast in the ADF image.

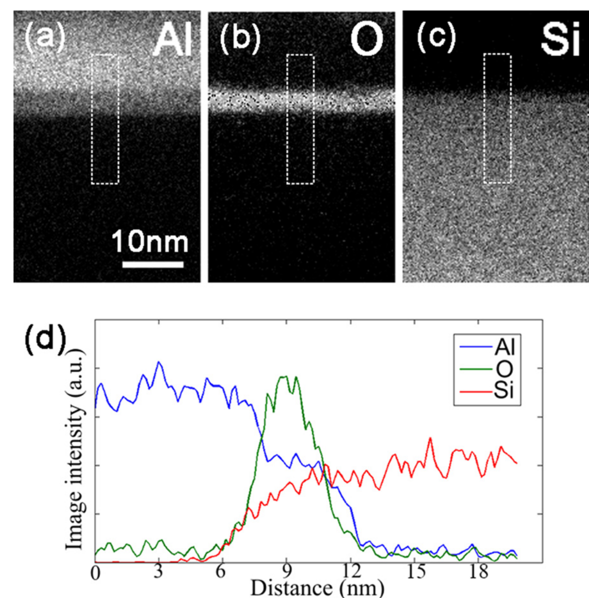

FIG. 2. EFTEM images acquired with Al L-edge (a), O K-edge (b), and Si L-edge (c) at the Al/Si interface region in the Al/AlO_x/Al junction. (d) Intensity profiles of the elemental maps of Al, O, and Si across the junction/substrate interfaces. The intensity profiles were measured within an area with a size of $\sim 5 \times 22\,nm^2$ and integrated along the direction parallel to the Al/Si interface. The areas where the intensity profiles were measured are marked in the EFTEM images of (a), (b), and (c).

evidenced from the O map shown in Fig. 2(b). Therefore, the interfacial layer consists of an intermixing of Al, Si, and O. Fig. 2(d) shows the intensity profiles measured in Figs. 2(a)–2(c) from the regions marked with white rectangles. The qualitative distribution of Al, Si, and O at the Al/Si interface region can be extracted from the profiles. In general, all three elements are distributed over the amorphous interface layer. There is more O at the center of the layer when compared to the interfaces close to the bottom Al layer and the Si substrate. The concentration of Si increases gradually in the interface layer from the bottom Al side to the Si substrate. It is possible that the HF etching of the Si wafer, before inserting it into the deposition chamber, was not enough to etch away the native SiO_2 on the surface of the Si wafer leaving a residual native oxide on the Si substrate. It is known that Al can reduce SiO_2 both at room temperature and elevated temperatures when Al thin films are deposited on SiO_2 substrates.[22–25] Al and Si interdiffusion is also a known phenomenon when fabricating metallic contacts for integrated circuits.[26] As a result, the intermixing among Al, Si, and O can happen during the Al film deposition via either a solid-state reaction between Al and SiO_2, implantation of Al into the substrate and the interdiffusion of Al and Si. The resulting interfacial structure may vary with the temperature of the substrate, the energy of the incoming Al atoms and/or clusters, and the thickness of the oxide layer.

The detailed structure of the material at the qubit/Si substrate interface was analyzed using spatially resolved STEM-EELS. In particular, energy loss near edge structure (ELNES) was used to study the characteristics of chemical bonding in the intermixed layer of Al, Si, and O, and the evolution of them across the interfaces with high spatial resolution. The result is shown in Fig. 3. The EEL spectra acquired in the energy loss range from ~70 eV to ~130 eV are shown in Fig. 3(a). The background of each spectrum was removed using a power-law model. Both the Al L_{23} edge and Si L_{23} edge are present in this energy loss region. Fig. 3(b) shows the interface area, where the STEM-EELS experiments were carried out. Sequential EEL spectra were recorded with a distance of ~0.35 nm between each point. The size of the electron probe is estimated to be around 0.13 nm. The line profiles acquired from different locations along the interface show the same characteristics, so in Fig. 3(a), we only show one of the line profiles acquired across the interfaces from bottom Al layer to Si substrate. From Fig. 3, we can clearly see that when the electron beam was positioned on the bottom Al layer and away from the interfacial layer, an edge arising at ~72.5 eV is the most dominant feature in the EEL spectrum (e.g., spectrum 1 in Fig. 3(a)). This edge is the Al L-edge from Al metal and is consistent with the spectrum of metallic Al in the literature.[27] As the electron beam moves into the interfacial layer between Al and Si (Area I), the edge at ~72.5 eV starts diminishing and shifts to ~75 eV. At the same time, two fine peaks at around 77.6 eV and 79.5 eV appear and become more and more profound (from spectrum 3 to spectrum 10). The presence of the edge starting at ~75 eV indicates the existence of an Al-O bonds and the disappearance of metallic Al bonds at the interface. In systems with Al-O bonding such as alumina and silicates, the structure of the material is usually characterized by the Al coordination. It is known that Al L_{23} ELNES is sensitive to the Al-O coordination state.[27–30] By comparing the recorded Al L_{23} ELNES to the reference spectra acquired from different polymorphs of alumina,[27] we find that the Al L_{23} ELNES we obtained within the interfacial layer (spectra 3–10) is identical to that from amorphous Al_2O_3. It is also consistent with the imaging and diffraction results mentioned above. In the amorphous Al_2O_3, the Al is predominantly tetrahedrally coordinated, which is evidenced by the presence of the fine peak at around 77.6 eV (labeled as "T" in Fig. 3(a)). The peak at around 79.5 eV (labeled as "O" in Fig. 3(a)) is characteristic of the Al sites with coordination number six. When the electron beam moves further towards the Si substrate (Area II), the Al L_{23} ELNES changes again. The peaks at 77.6 eV and 79.5 eV degrade gradually and finally disappear, whereas the edge starting from 75 eV is still visible (spectra 11–15). Meanwhile, the Si L-edge arising from ~100.5 eV emerges and becomes clearer, as electron beam moves closer to the Si layer (spectrum 14–20). Finally, when the electron beam moves into the Si layer, the signals from Al L-edge disappear completely, and Si L-edge from elemental silicon is the dominant feature in the EEL spectrum (spectrum 20). We note that there is no SiO_2 or silicate at the interfacial region because signals from Si-O bonding were not detected. Moreover, Al did not diffuse into the single crystalline Si substrate as indicated by the absence of Al EELS signal in the single crystalline Si substrate region. Most likely, Al reacts with the native silicon oxide remained on the Si surface, forming an interfacial layer comprised of aluminum oxide and Si, which is thermodynamically more favorable. The thin native oxide on the surface of Si

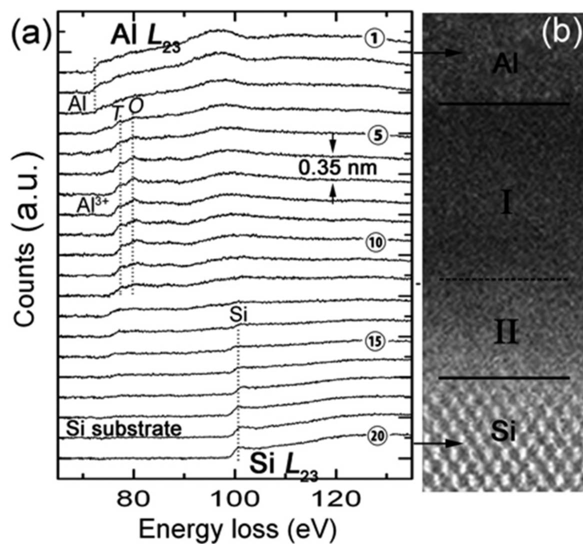

FIG. 3. (a) STEM-EELS spectra acquired across the junction/substrate interface from the bottom Al layer to the single-crystalline Si substrate region. The distance between two adjacent spectra is ~0.35 nm. The fine feature at 77.6 eV and 79.5 eV is marked with "T" and "O," respectively. Dashed lines marking the positions of different edges and peaks are drawn for clearance. (b) STEM ADF image showing the area where EELS spectra in (a) were acquired. The positions of spectrum 1 and spectrum 20 are indicated by the arrows.

substrate is also a barrier for the diffusion of Al into Si substrate.

Though the Si L-edge in Fig. 3(a) only becomes visible in spectra 15–20, the shift of the bump at around 95 eV (most visible in spectrum 1) towards the high energy direction comes from the overlap of Si L-edge on the Al L-edge, suggesting the presence of Si signals in spectra 3–14. This observation is in accordance with the distribution of Si shown in the Si elemental map in Figs. 2(c) and 2(d). Thus, both aluminum oxide and Si are distributed in the whole interfacial layer with a thickness of about 5 nm. Because of the overlap of the two edges, it is hard to quantify the concentration of the two components at the interface. However, qualitatively, from EFTEM (Fig. 2) and EELS (Fig. 3(a)) results, we can notice that the concentration of aluminum oxide decreases from the area close to Al to the area close to Si, i.e., from Area I to Area II. The concentration of Si shows the opposite trend. Furthermore, the Al L_{23} ELNES in spectra from 13 to 17 (Area II) is different from that in spectra from 4 to 12 (Area I). In the former region, distinct peaks in ELNES are not visible but Al L-edge from Al-O bonding still exists. While in the latter area, distinct peaks at 77.6 eV and 79.5 eV representing the structure of amorphous Al_2O_3 can be found. It suggests that in Area II, Al and O atoms are distributed more randomly, resulting in less modulation in the Al-*d* projected density of states in the conduction band. The distribution of aluminum oxide and Si and the different structures of the aluminum oxide found at different locations in the interfacial layer may give rise to the layered structure within the interfacial layer in STEM ADF images shown in Figs. 1(b) and 3(b). The solid-state reaction between bottom Al electrode in Al based Josephson junctions and SiO_2 substrates has been studied previously.[22] The reaction resulted in the formation of alumina and Si at the Al/SiO_2 interface, similar to the interaction at the Al/Si (HF treated) interface described in our study here. However, as revealed by ELNES, Al is tetrahedrally coordinated in the alumina formed at the Al/Si (HF treated) interface, while the alumina formed at the Al/SiO_2 interface shows a similar Al coordination to crystalline α-Al_2O_3, with Al being octahedrally coordinated. The difference in atomic structure of alumina formed at these two interfaces may be a result of the difference in stoichiometry of SiO_2 in the substrates. Thermally grown SiO_2 on Si is likely to be stoichiometric, whereas the native oxide on Si and the HF treated SiO_2 tends to be non-stoichiometric (oxygen deficient).[31] The deficiency in oxygen in SiO_2 at the Al/Si (HF treated) interface can give rise to a lower coordination number for Al in the alumina formed at the interface. It is also possible that the temperature difference at the substrate when depositing Al films for those two systems affects the atomic structure of the alumina at the interfaces. A more detailed investigation is needed to unveil the mechanism of the atomic structure difference of alumina at different types of junction/substrate interfaces.

IV. CONCLUSION

In conclusion, we have studied the structure at the interface between Al/AlO_x/Al Josephson junctions and Si substrates with the Si substrates being HF etched prior to film deposition. An interfacial layer with the thickness of about 5 nm comprised of amorphous aluminum oxide and elemental Si was found. Aluminum oxide and Si are both distributed in the whole interfacial layer, but their concentrations vary with position. The concentration of aluminum oxide in the interfacial layer decreases from the area close to bottom Al electrode to the area close to Si substrate, while the Si concentration increases, according to EFTEM images and EELS signals from Al L-edge and Si L-edge. Moreover, the Al-O bonding also changes with position. At positions close to the Al layer, the Al-O bonds show the characteristics of that in amorphous Al_2O_3, in which Al is mainly tetrahedrally coordinated, whereas in the region close to Si substrate, Al-O bonds with different characteristics are present. The variations may result in the layered structure within the interfacial layer as seen by STEM ADF imaging. The detailed structure provided by this study should be taken into account when modeling the interaction between the energy states in the qubit and the substrate. Our results add information of importance for the identification of the origin of decoherence in the superconducting quantum circuits and to the development of methods to diminish it. For example, in the system made from Al/AlO_x/Al Josephson junctions on Si substrate, the decoherence may originate from the defect states or TLF in amorphous aluminum oxide and Si, instead of SiO_2. To avoid this intermixing interfacial layer, ion milling of the substrate in the deposition chamber may be needed.

ACKNOWLEDGMENTS

We thank the Swedish Foundation for Strategic Research, the Swedish Research Council, and the Knut and Alice Wallenberg Foundation for financial support.

[1]M. A. Nielsen and I. L. Chuang, *Quantum Computation and Quantum Information* (Cambridge Univ. Press, Cambridge, U.K., 2000).
[2]J. Q. You and F. Nori, Phys. Today **58**(11), 42 (2005).
[3]R. J. Schoelkopf and S. M. Girvin, Nature **451**, 664 (2008).
[4]M. H. Devoret and R. J. Schoelkopf, Science **339**, 1169 (2013).
[5]A. A. Houck, H. E. Türeci, and J. Koch, Nat. Phys. **8**, 292 (2012).
[6]Y. Makhlin, G. Schön, and A. Shnirman, Rev. Mod. Phys. **73**, 357 (2001).
[7]A. O. Niskanen, K. Harrabi, F. Yoshihara, Y. Nakamura, S. Lloyd, and J. S. Tsai, Science **316**, 723 (2007).
[8]M. D. Reed, L. DiCarlo, S. E. Nigg, L. Sun, L. Frunzio, S. M. Girvin, and R. J. Schoelkopf, Nature **482**, 382 (2012).
[9]A. Lupaşcu, E. F. C. Driessen, L. Roschier, C. J. P. M. Harmans, and J. E. Mooij, Phys. Rev. Lett. **96**, 127003 (2006).
[10]Y. A. Pashkin, T. Yamamoto, O. Astafiev, Y. Nakamura, D. V. Averin, and J. S. Tsai, Nature **421**, 823 (2003).
[11]M. Steffen, M. Ansmann, R. C. Bialczak, N. Katz, E. Lucero, R. McDermott, M. Neeley, E. M. Weig, A. N. Cleland, and J. M. Martinis, Science **313**, 1423 (2006).
[12]T. Hime, P. A. Reichardt, B. L. T. Plourde, T. L. Robertson, C.-E. Wu, A. V. Ustinov, and J. Clarke, Science **314**, 1427 (2006).
[13]A. Fay, E. Hoskinson, F. Lecocq, L. P. Lévy, F. W. J. Hekking, W. Guichard, and O. Buisson, Phys. Rev. Lett. **100**, 187003 (2008).
[14]J. Clarke and F. K. Wilhelm, Nat. Phys. **453**, 1031 (2008).
[15]G. Ithier, E. Collin, P. Joyez, P. J. Meeson, D. Vion, D. Esteve, F. Chiarello, A. Shnirman, Y. Makhlin, J. Schriefl, and G. Schön, Phys. Rev. B **72**, 134519 (2005).

[16]J. M. Martinis, K. B. Cooper, R. McDermott, M. Steffen, M. Ansmann, K. D. Osborn, K. Cicak, S. Oh, D. P. Pappas, R. W. Simmonds, and C. C. Yu, Phys. Rev. Lett. **95**, 210503 (2005).
[17]C. Rigetti, J. M. Gambetta, S. Poletto, B. L. T. Plourde, J. M. Chow, A. D. Córcoles, J. A. Smolin, S. T. Merkel, J. R. Rozen, G. A. Keefe, M. B. Rothwell, M. B. Ketchen, and M. Steffen, Phys. Rev. B **86**, 100506(R) (2012).
[18]R. Barends, J. Kelly, A. Megrant, D. Sank, E. Jeffrey, Y. Chen, Y. Yin, B. Chiaro, J. Mutus, C. Neill, P. O'Malley, P. Roushan, J. Wenner, T. C. White, A. N. Cleland, and J. M. Martinis, Phys. Rev. Lett. **111**, 080502 (2013).
[19]M. Stern, G. Catelani, Y. Kubo, C. Grezes, A. Bienfait, D. Vion, D. Esteve, and P. Bertet, Phys. Rev. Lett. **113**, 123601 (2014).
[20]J. M. Martinis, S. Nam, J. Aumentado, and C. Urbina, Phys. Rev. Lett. **89**, 117901 (2002).
[21]S. K. Choi, D.-H. Lee, S. G. Louie, and J. Clarke, Phys. Rev. Lett. **103**, 197001 (2009).
[22]L. J. Zeng, T. Greibe, S. Nik, C. M. Wilson, P. Delsing, and E. Olsson, J. Appl. Phys. **113**, 143905 (2013).
[23]R. S. Bauer, R. Z. Bachrach, and L. J. Brillson, Appl. Phys. Lett. **37**, 1006 (1980).
[24]F. Dadabhai, F. Gaspari, S. Zukotynski, and C. Bland, J. Appl. Phys. **80**, 6505 (1996).
[25]S. M. Goodnick, M. Fathipour, D. L. Ellsworth, and C. W. Wilmsen, J. Vac. Sci. Technol. **18**, 949 (1981).
[26]L. J. Brillson, M. L. Slade, A. D. Katnani, M. Kelly, and G. Margaritondo, Appl. Phys. Lett. **44**, 110 (1984).
[27]D. Bouchet and C. Colliex, Ultramicroscopy **96**, 139 (2003).
[28]K. Kimoto, Y. Matsui, T. Nabatame, T. Yasuda, T. Mizoguchi, I. Tanaka, and A. Toriumi, Appl. Phys. Lett. **83**, 4306 (2003).
[29]R. Brydson, J. Phys. D: Appl. Phys. **29**, 1699 (1996).
[30]P. L. Hansen, R. Brydson, D. W. McComb, and I. Richardson, Microsc. Microanal. Microstruct. **5**, 173 (1994).
[31]D. Graf, M. Grundner, R. Schulz, and L. Muhlhoff, J. Appl. Phys. **68**, 5155 (1990).